J Mater Sci (2007) 42:5036–5045
DOI 10.1007/s10853-006-1403-y

Characterization and mechanical behavior of ceramic rings

A. G. Tomba Martinez · M. M. Reboredo · A. L. Cavalieri

Received: 13 April 2005 / Accepted: 22 February 2006 / Published online: 23 February 2007

Abstract Diametral compression is usually used to determine the mechanical resistance of cylindrical ceramic specimens. This work deals with the possibility of employing diametral compression in order to evaluate the mechanical response of ceramic rings, by testing two sets of rings (used as pump seals) that had two different sizes. The rings were characterized by different techniques: qualitative X-ray diffraction, apparent density and porosity measurements, determination of Vickers hardness, surface roughness, and microstructural analysis. α-alumina was identified as the majority crystalline phase in both types of rings. The porosities were rather similar, even though the observed mean grain size of the large rings was slightly larger. Significant differences were observed in the average roughness. Diametral compression tests at room temperature were carried out on a statistical number of each ring set. The fracture features were analyzed by ocular inspection and SEM observation of the fracture surfaces. Several approaches were used to estimate the fracture strengths: three analytical formulae with and without an empirical constant, and a finite element calculation. The simplest approach, an analytical formula that only requires the knowledge of the geometrical magnitudes of rings besides de fracture loads, gave a conservative estimation of the mechanical strength of rings and a limited explanation of fracture features. On the other hand, the numerical model being the most complex and informative of the approaches, gave the complete stress distributions.

A. G. Tomba Martinez (✉) · M. M. Reboredo · A. L. Cavalieri
Instituto de Investigaciones en Ciencia y Tecnología de Materiales (INTEMA), UNMdP – CONICET, Av. J.B. Justo 4302, 7600 Mar del Plata, Argentina
e-mail: agtomba@fi.mdp.edu.ar

Introduction

The mechanical resistance of cylinders is commonly evaluated by diametral compression [1–4]. This method is based on the developed stresses when the specimen is compressed between two diametrically opposite loads. Although less frequently, diametral compressive loading of circular rings is also applicable to the measurement of tensile properties of brittle materials [5, 6]. The advantages of this test include greater consistency and simplicity.

A circular ring of rectangular cross-section is probably the most commonly treated geometrical shape in stress analysis literature [7]. The application of diametrically opposite outer loads is the most utilized loading condition in that shape [8]. Applications of this form are numerous since this type of rings is the transverse cross-section of tubes widely used in construction. This geometrical shape, moreover, is common in commercial ceramic mechanical seals with more or less complex shapes according to their function [9, 10] in revolving or stationary parts. This is due mainly to a high service security, low or null maintenance, minimum losses, and long duration. These shapes have an exceptionally extensive range of applications, most importantly shown in the sectors of appliances, car industry, chemical, petrochemical, aeronautical, space industries and industrial, and agricultural pumps.

This work is focused to the characterization of available commercial ceramic rings used as pump seals and the study of their mechanical behavior. Rings of two different dimensions were characterized using several techniques and mechanically tested by the simpler diametral compression method. Furthermore, four approaches were used to estimate the fracture strengths: a finite element based calculation and three analytical formulae, one based on an analysis for thin rings [11], a second one including an empirical parameter [5], and the last one considering a theoretical stress constant [8]. A comparative discussion of these estimations was carried out.

Experimental

Materials

Ceramic commercial rings used as pump seals of two sizes labeled small (S) and large (L), respectively, were characterized and mechanically tested. Their dimensions (R_o = outer diameter, R_i = inner diameter, b = width) are shown in Table 1. Different surface finishes were observed by visual inspection of the rings: (a) shiny and dull flat surfaces that correspond to the ceramic/ceramic (side 1) and the ceramic/O-ring (side 2) arrangements in mechanical seal, respectively, and (b) similar inner and outer circular surfaces, with more dullness than side 2.

Characterization

The qualitative analysis of crystalline phases present in rings was carried out by X-ray diffraction (XRD) using a Philips equipment PW 1830 (CuK_α radiation; Ni-filtered, at 40 kV and 30 mA).

Microstructures of rings were analyzed by scanning electron microscopy (SEM), using a Philips 505 microscope, on shiny surface thermally etched (1,550 °C, 30 min) to reveal the grains. EDAX analysis was simultaneously carried out. Mean grain size (D_{50}) was measured using the Image Pro image analyzer program.

Table 1 L and S ring dimensions (R_o = outer diameter, R_i = inner diameter, b = width)

	L	S
R_o (mm)	18.01 ± 0.02	6.37 ± 0.02
R_i (mm)	10.24 ± 0.02	4.11 ± 0.02
R_o/R_i	1.76 ± 0.02	1.55 ± 0.02
b (mm)	6.02 ± 0.02	5.05 ± 0.02

Pycnometric densities (ρ_{pic}) of the powders obtained by crushing the rings to 70-mesh (<210 μm) were determined in kerosene at 37 °C. Apparent densities of rings (ρ_{app}) were determined by Archimedes method in water at room temperature. The glass content (g) was estimated using the pycnometric density of each ring and the theoretical density of the main phase identified by XRD. On the other hand, the composition of the glassy phase was estimated based on the SEM/EDAX analysis. Considering these data, a density value for a glass with this composition was taken from literature. In turn, the ring porosities (p) were calculated relating the pycnometric and the apparent densities.

The surface features of sides 1 and 2 were observed by reflection optical microscopy using a metalographic microscope Olympus PMG3 at 1000X without immersion.

The average roughness of the four ring surfaces (R_a) was measured with a Surtronic 3+ (Taylor Hobson) surface profilometer equipped with a 1 μm diamond stylus tip. A traverse length of 1.25 mm and a cut-off length of 0.25 mm were used.

The Vickers hardness (H_v) was determined on the shiny surface of ''as received'' rings by the indentation technique using a Tukon 300 microhardness tester at indentation load of 2.5 kg during 15 s.

Mechanical evaluation

Test

In order to evaluate the ring mechanical strengths, the fracture load was determined in a diametral compression test. The specimen was compressed between two diametrically opposite loads until its failure. A servo-hydraulic universal testing machine Instron 8501 with high load frame stiffness was used. The tests were carried out in air at room temperature using steel loading platens.

Preliminary tests were performed to determine the experimental conditions to be used. A thin pad of a suitable material was placed between the specimen and the hard platens to reduce the concentration of compressive and shear stresses at the loading points and to distribute the load properly [3]. Also, the pad reduced the friction in the contact area, which could have led to a higher apparent tensile strength [3]. Three different pad materials were tested: a copper sheet (0.115 mm in thickness), and lithium and MoS_2 pastes, being the last material selected because it achieved the best quality of contact. When copper was employed, a high deformation of the sheet and a bad contact area were observed.

In addition to the pad, very thin sheets of both white and carbon papers were placed between the ring and the pad on top and bottom of the specimen. After the test, the paper marks were used to get an estimation of the quality of the contact area.

Several rates from 0.01 mm/min to 0.5 mm/min were tried so it was possible to select the same displacement speed of 0.05 mm/min for both sizes of rings. For higher rates, the fracture times below 1 min were too short and the load–displacement curve was never linear. So, it was possible that the specimen appropriate setting would not be achieved for a reliable testing. Moreover, a bad contact between the sample and the platens with paper rupture occurred. Conversely, lower rates produced too long test times (>5 min). In this condition, slow crack growth previous to unstable propagation would be even more likely to occur.

The features of the ring fracture were analyzed. The fracture sequences were visually determined during the test and the fracture surfaces were observed by SEM (Philips 505 microscope) in an attempt to identify the origin and/or the mode of fracture.

Fracture strength estimation

The fracture strengths (σ_F) of the rings were obtained from the measured fracture loads using four approaches: (a) three analytical formulae derived on the basis of assumptions about the stress distribution in the system and (b) a finite element calculation for the stress distribution. A simple failure criterion was considered: the fracture occurs when the local stress at the point of maximum tensile stress reaches the material ultimate strength.

A statistical analysis of σ_F values estimated from every approach was carried out. The failure probability estimator $P_F = (i - 0.5)/N$, appropriate for the employed population size, was used to report the results as distribution curves.

(a) Analytical calculi

The stress distribution in a diametrically loaded ring is complex. However, several analyses of this geometry have been done using simplifying assumptions [5–8, 11, 12]. The system is generally treated as a two-dimensional problem and the elasticity theory is used. These analyses localize the point subjected to maximum tension and give analytical expressions that include, in some cases, empirical or theoretical constants related to the stress concentration.

Three analyses were considered to determine the values of ring strengths: Calculus (1) an analytical formulae derived from that proposed by Roark [11] for thin rings (radius >> radial thickness); Calculus (2) an expression developed by Frocht [12] that includes an empirical stress constant determined for several materials by Bortz and Lund [5], and Calculus (3) an universal expression derived by Durelli and Lin [7].

(a1) Calculus 1

Roark [11] estimated the maximum tensile stress (σ_{MAX}) that happened to occur at loading points, by considering the ring as a statically indeterminate beam and assuming that: (a) the ring section was uniform, (b) in comparison with its radial thickness the ring radius was so large that the deflection theory for straight beam was applicable, (c) its deflection was due solely to bending (direct axial tension or compression, and shear, were negligible), (d) it was nowhere stressed beyond the elastic limit and (e) the ring was not severe deformed so it maintains its essentially circular shape. It is considered that both types of rings studied here, L and S, fulfill the restrictions even when the radial thickness was not too small in comparison with R_o (h/R_o are 0.43 and 0.35 for L and S, respectively). Taking this fact into account, a related expression for the maximum tensile stress was derived (Eq. 1) taking the ring radius (R) as the mean value between the outer and inner ones (R_o and R_i, respectively):

$$\sigma_{MAX} = \frac{1.9098\,PR}{bh^2} \tag{1}$$

where $h = (R_o - R_i)$ is the radial thickness, b is the width, and P is the applied load; σ_{MAX} is the fracture strength σ_F when P is the fracture load.

It should be noted that this estimation of mechanical strength only uses ring dimensions and experimental load of fracture. The complete analysis also would give the value of stress at different points of the ring [11] (although it does not distinguish between inner and outer boundary).

(a2) Calculus 2

Using Frocht solution of the problem [12], Bortz and Lund [5] proposed an estimation of the ring stress failure based in a semi-empirical equation (Eq. 2):

$$\sigma_F = 2\frac{PK^B}{(R_o - R_i)b} \tag{2}$$

where K^B is a stress constant experimentally determined which requires the use of strain gages during the mechanical test [5]. This formulae was derived considering that the maximum tensile stress was developed on the inner periphery of the ring at the load axis.

The value of stress components at other points in the ring could be obtained if the mathematical complications would be surmounted.

(a3) Calculus 3

Durelli and Lin [7] gave the stresses in a ring subjected to two diametrically opposite loads. The values for all the points at the inner and outer boundaries were presented using the ratio of radius (R_i/R_o) as a parameter. A universal expression of stress (σ_θ) as a function of the angular position θ was derived (Eq. 3):

$$\sigma_\theta = \frac{PK^D}{\pi R_o b} \tag{3}$$

where K^D is a universal stress constant that depends on R_i/R_o value (and θ, of course) but not on the material. This value was obtained theoretically by Durelli using six terms of the numerical series employed to express stresses [7]. As in the previous calculus, the results are limited to elastic behavior of materials and small deformation of rings.

For the calculus of the strength using Eq. 3, points of maximum tensile stress were identified (inner or outer boundary and angular position) and the values of K^D were taken from Durelli plots [7] using the value of R_i/R_o ratio for L and S rings, respectively.

(b) Finite element calculus

Finite element analysis (FEA) is a powerful tool to resolve structural problems because complete distributions (spatial and temporal) of strain and stress in the specimen can be obtained. Additionally, many different supports and loading conditions can be used in the calculus and they can be modified step by step in order to improve the numerical model, i.e., to increase the similarity with the real system and obtain better results.

A numerical calculation using a finite element method was carried out as a more realistic model to evaluate the ring mechanical strength. A commercial code LUSAS version 13.4 was employed for calculations. The same material, boundary, and loading conditions were considered for both, L and S, rings. The material was assumed as elastic, linear, and isotropic. As a first approach to the problem, only a quarter of the ring was simulated as a bidimensional problem because of the specimen and the loading configuration symmetry. For stress calculations, a plane deformation problem was considered and a concentrated load distributed over the ring width was used. Equivalent regular meshes were designed for both types of rings with 800 linear square elements. Nodes at both radial boundaries were restricted to move (null displacement) along their normal direction.

The stress profile could be obtained in overall domain, not only the ones at the boundaries, but a complete stress distribution was attained. The identification of points of maximum tensile stress was carried out in order to determine the distribution curves of the mechanical strength for both sizes of rings.

Results and discussion

Characterization

The diffraction patterns did not show significant variation between the different types of rings. α-alumina (corundum ICDD 42-1468) was identified as the majority crystalline phase.

SEM micrographs of thermal etched shiny surfaces (side 1) for both types of rings are shown in Fig. 1.

The microstructures were homogeneous with mainly equiaxial grains. The mean grain size determined by the micrographs image analysis (D_{50}, Table 2) was slightly larger for L rings than for S ones. The differences between pycnometric and apparent densities in L and S rings could be associated to the presence

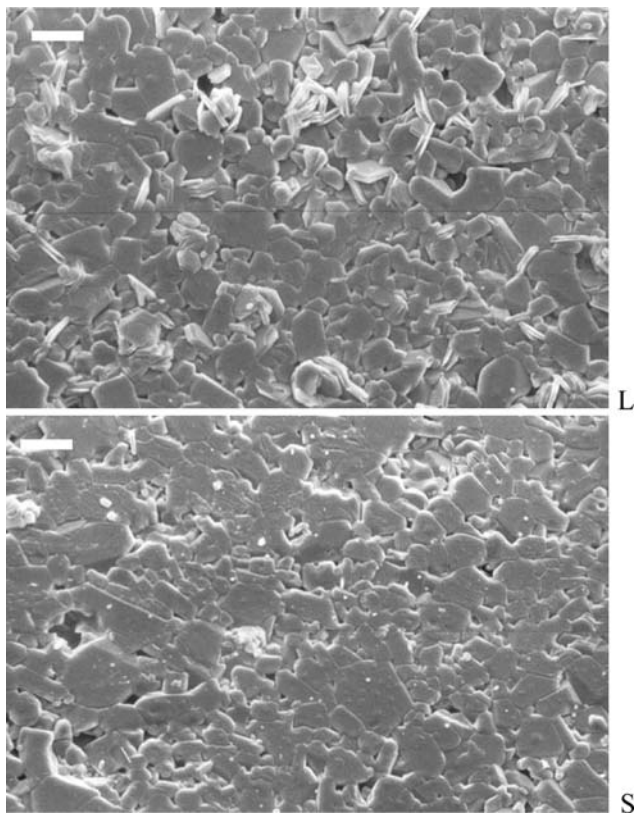

Fig. 1 SEM micrographs of thermal etched surfaces of ring shiny side. Scale bar: 20 μm

Table 2 Main characteristics of L and S rings (ρ_{pic} = pycnometric density, ρ_{app} = apparent density, g = glass content, p = porosity, R_a = average roughness, D_{50} = mean grain size, H_v = Vickers hardness)

Crystalline phase		L	S
		α-Al_2O_3 (corundum)	
ρ_{pic} (g/cm^3)		3.77 ± 0.05	3.83 ± 0.06
ρ_{app} (g/cm^3)		3.64 ± 0.03	3.61 ± 0.01
g (%)		14 ± 2	10 ± 1
p (%)		3.5 ± 0.5	3.8 ± 1.0
R_a (μm)	Side 1	0.65 ± 0.01	0.24 ± 0.09
	Side 2	0.75 ± 0.14	0.74 ± 0.03
	Inner side	1.12 ± 0.03	1.63 ± 0.08
	Outer side	1.86 ± 0.56	1.88 ± 0.44
D_{50} (μm)		7.6 ± 1.6	6.7 ± 1.8
H_v (GPa)		8.8 ± 1.7	9.3 ± 1.5

of pores. The observed total porosities of L and S rings were rather similar between them in concordance with the estimated values of p% (Table 2) and the mean pore sizes were closer to the respective grain ones. It is worthy to note that a few large pores of about 20–30 μm were also exhibited in both pore size distributions. A glassy phase, which was expected to be present in commercial sintered products as the studied alumina rings, was observed in triple points.

Aluminum was determined by EDAX analysis in crystals of both L and S rings in which Al_2O_3 was the main phase. The detection of Si (10–15 wt%) and Ca (15–20 wt%) in the zones where grains boundaries prevail could be taken as an indication of the presence of a calcium silicate glassy phase. A density equal to 2.5 g/cm^3 [13] for the last phase was considered in order to estimate its content (g%, Table 2) in L and S rings. A somewhat higher amount of glass was inferred in L rings. However, g values could only be considered as a guide due to the assumptions used in their estimations.

In L rings as well as in S ones, significant differences were observed in the average roughness (R_a, Table 2) measured in the inner and outer sides, higher than those exhibited on sides 1 and 2. It could also be noticed that between L and S rings there were no appreciable differences in the values obtained on side 2 and inner or outer sides. Nevertheless, the difference was very noticeable in side 1, the shiny surface: a rougher surface was present in L rings. This fact agrees with the observations carried out by optical microscopy (not shown) regarding the quality of surfaces. These differences could be explained if the values of R_a for these alumina rings are compared with different alumina materials reported in the literature [14, 15] and if the forming methods commonly used for this type of geometry (roll compaction tape, dry pressing, extrusion) are considered. It can be inferred that no further grinding treatment was performed on inner and outer sides of L and S rings after the forming/sintering steps. Moreover, a coarse grinding (>120 or 70 grit) and a finer one (<120 or 325 grit) could be carried out on side 2 and side 1, respectively. Considering the relative low value of roughness for side 1 in S rings, a coarse polishing cannot be discarded in this case in addition to the influence of the slightly lower mean grain size of S rings.

The Vickers hardness measured on L and S rings (H_V, Table 2) showed no significant difference between them. However, they were lower than those reported for dense alumina (≈16–18 GPa [16, 17]). A correction to zero porosity can be done using the relation [18]:

$$H_v = H_v^0 \exp\ (-cp) \tag{4}$$

where H_v^0 is the hardness for $p = 0$ and c is an empirical constant. Using $c = 3$ for alumina [19], the mean hardness for L and S rings increases up to 9.8 GPa and 10.4 GPa, respectively. However, the consideration of the contribution of the porosity does not justify the whole difference with the values reported. An explanation could be found in a decrease of the hardness due to the contribution of the silicate glassy phase, that also accounts for the lower value of H_v^0 in L rings.

Consistently with this fact, Sglavo et al. reported a similar value of hardness, 10.4 ± 0.6 GPa, for an alumina with 10% of intergranular glass [20].

Since the seals were not prepared in the laboratory but commercially fabricated, the use of several techniques to characterize the ceramics rings was necessary to give complementary information about both, internal and superficial, microstructures of the materials useful for their mechanical evaluation.

Mechanical evaluation

Fracture features

Typical load–displacement curves for both sizes of rings are shown in Fig. 2a and b (the displacement corresponds to the variation of the machine actuator position).

The first non-linear portion was mainly related to the arrangement of the specimen between the load platens since a high stiffness machine was used. In general, a linear response was achieved about the half

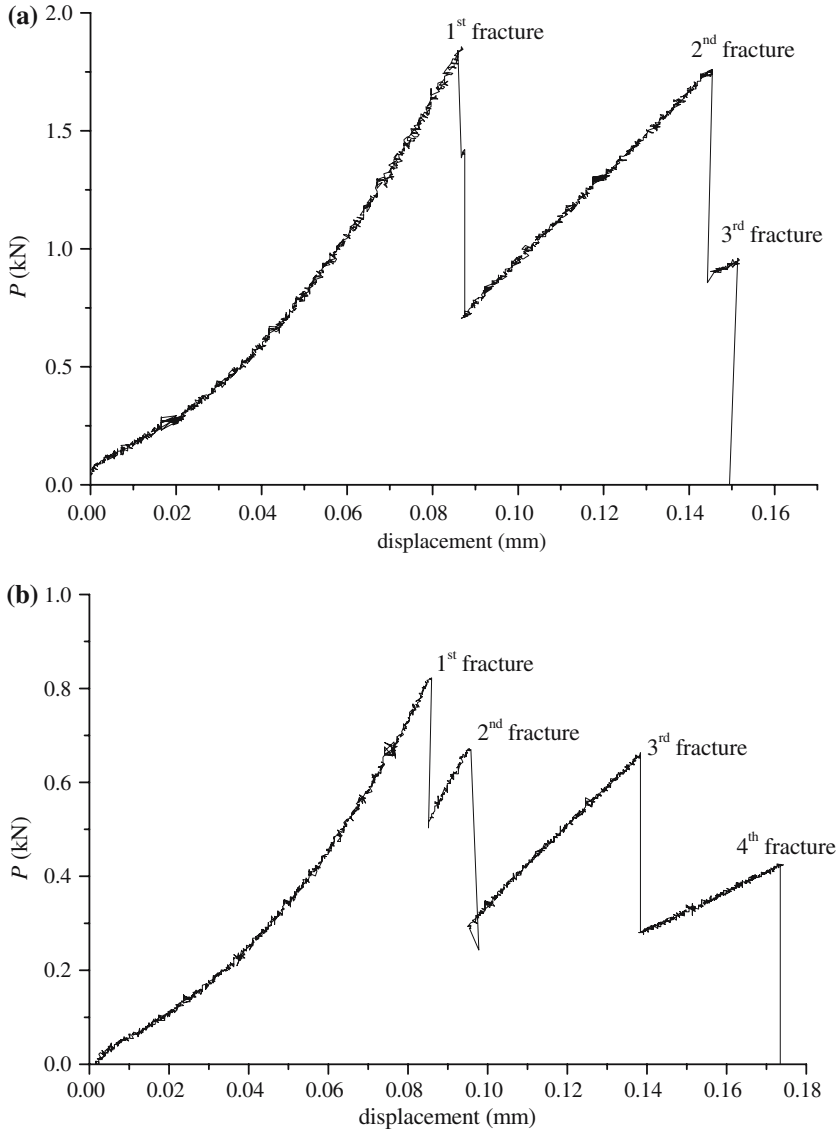

Fig. 2 Load–displacement curves: (**a**) L; (**b**) S. (P = load)

of the mean fracture load (≈1 kN for L and ≈0.4 kN for S).

The failure was similar for both sets of rings: it was always brittle but more than one crack occurred, similar to those reported in the literature [5]. The fracture, in every case, was initiated at the point where the load was applied (principal cracks). When a delay between the fracture at the top and the bottom was detected, the localization of the first one was random. The cases that showed fracture occurring simultaneously in both points were more frequent for rings that support higher loads and this fact could be associated to a higher stored energy at breakage.

The number of fragments and its distribution for L and S rings are reported in Table 3. The majority of rings exhibited one or two lateral cracks (i.e., the rupture of a C-ring) after the rupture at the load axis. The orientation of such secondary cracks with respect to the load axis was in the range 60–120°, being more frequent the rupture at 90° in S rings. In these rings, the crack paths were rather straight with flat fracture surfaces, while this situation in L ones was less frequent and the fracture surfaces exhibited ridges.

Table 3 Fragmentation features of L and S rings

	Number of fragments	Percentage	Secondary cracks at 90°
L	4	81%	29%
	3	13%	
	2	6%	
S	4	90%	42%
	3	10%	

For both L and S rings, similar features could be observed in the fracture surface images obtained by SEM at different magnifications (Fig. 3a–d). Based on the ring characterization, it was inferred that the inner or superficial pores arising in the processing as well as superficial flaws originated during forming (inner and outer sides) or grinding (sides 1 and 2), could act as fracture origin. In particular, based on roughness considerations, flaws at inner/outer surfaces would be more prone to initiate the rings failure. Since the glassy phase was mainly observed at triple points, it was considered that it was improbably that the fracture originated there. However, neither in L nor in S ring was it possible to identify the fracture origins by fractographic analysis. So, it was not possible to clarify the type of defect controlling the mechanical resistance of rings, or to identify in which side the fracture initiation was located.

Both, transgranular and intergranular modes of failures were observed, even though it resulted very difficult to evaluate the contribution of each fracture mode. No differences in fracture modes were observed between L and S rings probably due to the similarities in their mean grain size, although an increase in the intergranular failure could be expected with increasing grain size in Al_2O_3 [21].

Fracture strength estimation

The load value at the first peak of the curve (principal crack) was considered to estimate the fracture strength. The tested ranges of compressive loads at fracture were the following: 1.425–2.429 kN for L rings and 0.527–1.028 kN for S ones.

To estimate the mechanical strength of L and S rings, it was considered that the fracture initiated where the maximum tensile stresses occurred. Figure 4 and Table 4 show the fracture strength distribution curves and arithmetic mean σ_F values obtained from each model for both series of rings, respectively.

The localization of fracture initiation (principal cracks) in every model, taken as the position where the calculated maximum tensile stress occurred, was supported by the observation of the failure of L and S rings during the tests.

In most of the approaches, the slightly lower mechanical strengths calculated for L rings, which

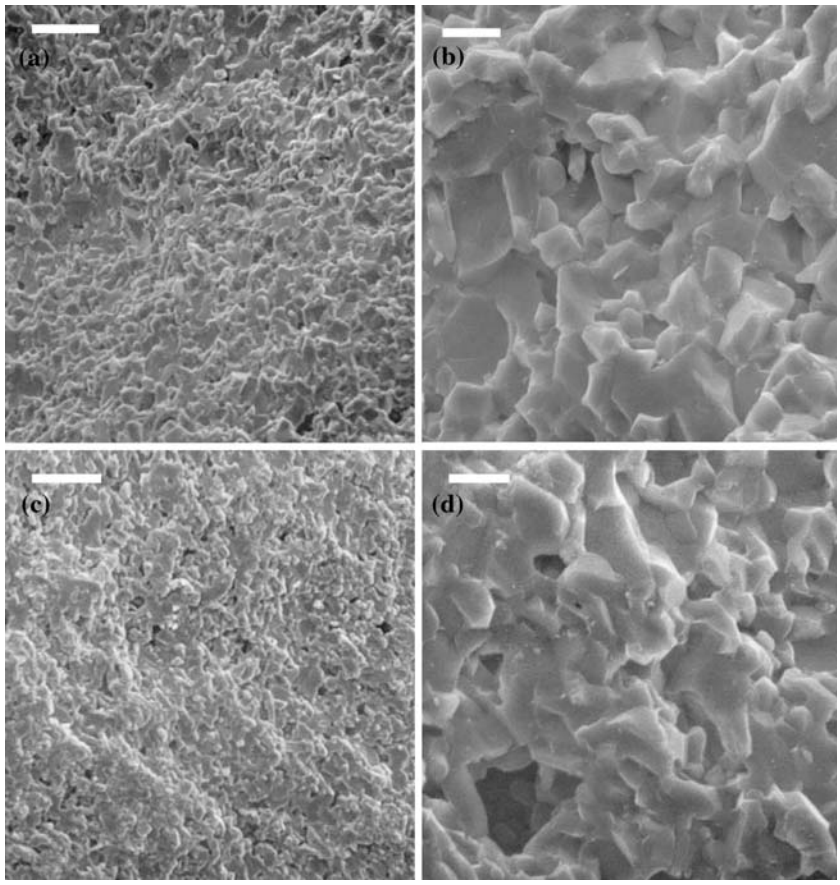

Fig. 3 SEM micrographs of fracture surfaces: (**a**, **b**) L and (**c**, **d**) S. Scale bars: (**a**–**c**) = 50 μm; (**b**–**d**) = 10 μm

Table 4 Arithmetic mean fracture strength (MPa)

Calculus	L	S
1	154 ± 23	167 ± 29
2	194 ± 30	207 ± 36
3	173 ± 27	169 ± 30
Numerical	337 ± 52	358 ± 63

had larger volume under the maximum tensile stress than S ones, could be accounted for by the Weibull statistical theory [22]. It states that larger critical flaws are more likely to be found in larger volumes of material.

In every strength distribution curve, the specimens with the lower fragmentation (Table 3) were more frequent at the region of lower fracture loads (and lower σ_F values) for both, L and S rings. This fact could also be associated to the lower amount of stored energy at the fracture onset.

(a) Analytical calculi

(a1) Calculus 1

It was derived from Roark analytical model [11] that the maximum tensile stress occurs at loading points. The values of σ_F obtained from Eq. 1 (Fig. 4 and Table 4) resulted in the order of those obtained for 95–97% Al_2O_3 cylinders tested in diametral compression [3] but lower than those reported for alumina rings [5] and for dense high purity alumina tested otherwise [6, 23–25].

(a2) Calculus 2

The values of K^B for alumina rings given by Bortz [5] with the corresponding R_i/R_o ratio were used for the calculus of strength (Eq. 2).

As it was previously established, this model stated that the maximum tensile stress was developed on the inner periphery of the ring at the load axis. Only the localization of fracture initiation (principal cracks) at the load axis was supported by observation on L and S rings failures, since the real origin of fracture was not identified in any case. The mechanical strengths (Fig. 4 and Table 4) estimated using Eq. 2 (with K^B values of 8.8 and 11.5 [5] for L and S rings, respectively) were higher to those obtained from Roark calculus (about 25% for both types of rings). Nevertheless, they were not enough to match the reported values. The same ratio between the mean values of σ_F for L and S rings was obtained.

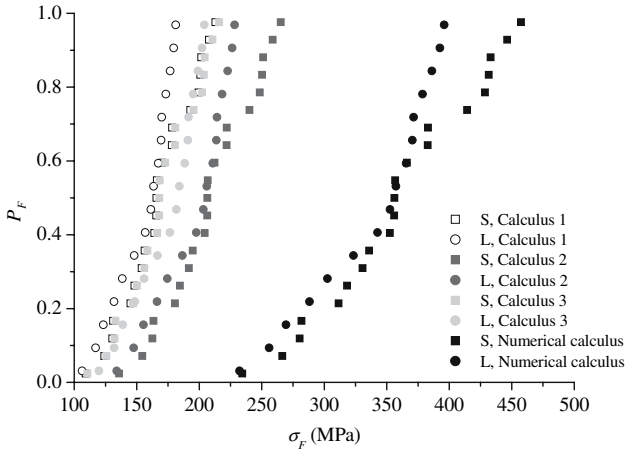

Fig. 4 Mechanical strength distribution curves (P_F = failure probability, σ_F = mechanical strength)

(a3) Calculus 3

It was inferred from Durelli plots [7] that the maximum tensile stress occurred on the inner periphery of the ring at the load axis ($\theta = 0°$), as in the previous model. Besides, a second maximum in tensile stress appeared at a normal axis ($\theta = 90°$) on the outer boundary that caused the secondary crack opening.

The values of mechanical strengths (Fig. 4 and Table 4) were intermediate between those estimated using Calculus 1 and 2. However, conversely to both models, the use of Durelli calculus gave similar values of σ_F being them slightly higher for L rings. The explanation to this fact has to be found in the different approximations used to obtain each solution. However, based in the results obtained by Bortz with different materials, the effect of the material in the stress constant that is dismissed in Durelli model should not be a factor to take into account for the difference.

(b) Numerical calculus

The Young modulus (373.750 GPa at room temperature) and the Poisson's ratio (0.26) for a 99.9% Al_2O_3 were taken from literature [16].

(b1) Stress profiles

Figure 5 shows the complete stress distributions calculated for L rings using the maximum compressive load at fracture (2.429 kN) for components σ_x and σ_y. Because of the assumptions of the model, the stresses along the ring thickness were uniform. For S rings, similar stress distributions were obtained, but with different absolute values. Using the same load, the stress values calculated for smaller rings were slightly higher than those obtained for L ones as the tendency obtained with calculi 1 and 2.

From the complete stress distribution, areas of high tensile stresses could be identified. The maximum tensile stress for σ_x was at the load axis on the inner diameter, while for σ_y component, it was at the perpendicular axis on the outer diameter. However, the value of x-component was higher than y-component, so it could be expected that the specimen failure began at the load axis, as it occurred. These results are coincident with those obtained from Durelli analyses.

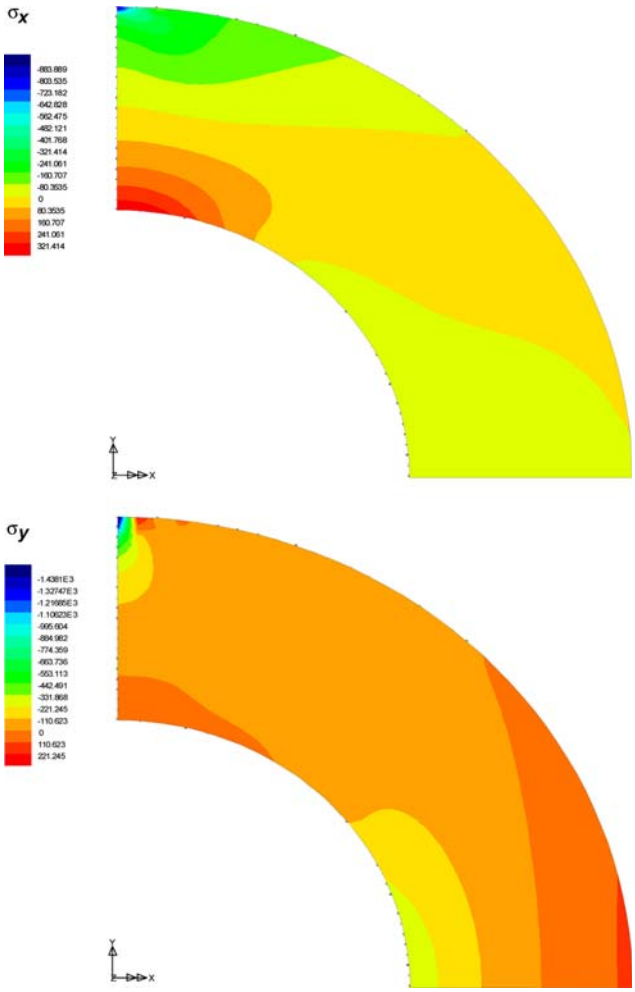

Fig. 5 Stress profiles for L ring using the maximum compressive load at fracture (σ_X = x-stress component, σ_y = y-stress component)

As in that case, no experimental support can be given about the point where the failure began since it was neither detected during the test, nor inferred from the fractography analyses whether the fracture initiated at the inner or at the outer diameter. The localization of the area of maximum tensile stresses in y-direction allowed to explain the presence of secondary cracks at 60–120° of the load axis.

(b2) Mechanical strength distributions

Figure 4 also shows the σ_F distributions curves obtained from numerical calculus using the experimental load of rupture and the maximum tensile value of σ_x. The mean values are reported in Table 4. Conversely to that values obtained using the analytical calculi (1–3), these fracture strength values resulted rather higher than the ones obtained by analytical calculi (about 73% of those of Calculus 3) and similar to those of high purity dense alumina [18, 21–22]. Although the numerical model includes some common assumptions and simplifications, the results were quite different to those from analytical approaches. Having in mind the microstructural characteristic of the rings, it was considered that their mechanical strengths were overestimated by numerical calculus.

(c) Comparative analysis

A location of fracture initiation (principal cracks) that was supported by the empirical evidence was obtained from the approaches used to estimate σ_F for L and S. The models, which gave more information for fracture features were Calculus 3 and finite element analyses.

The four approaches used to estimate σ_F for L and S rings gave different numerical results, although those of analytical calculi were grouped around lower and more differentiated values than those of numerical one. Lower mechanical strengths were estimated for L rings, in accordance with Weibull theory predictions, except with Calculus 3. Comparing analytical calculi, the lesser the simplifications used, the higher the calculated σ_F values were, reaching those of finite element analyses. Taking into account the rings characteristics and the literature values for alumina materials of similar quality, it was considered that more realistic values of σ_F would be intermediate between those estimated by Calculus 2 and numerical one. Calculus 1 underestimated the rings mechanical resistance and did not distinguish if the fracture initiated on the inner or on the outer ring boundaries. It still had the main advantage for being such simple as an analytical formula that only required the geometrical magnitudes of the rings, giving a conservative estimation of their mechanical strength. The other two analytical approaches were considered better models for the problem. It is believed that since Calculus 2 made use of material parameters, it gives a more realistic value of σ_F. However, this could also be an inconvenient since it requires additional experimental labor (the use of strain gages and the determination of experimental Young modulus). This is not necessary if Durelli plots (Calculus 3) are employed for the mechanical resistance estimation. Moreover, this analysis gives a better characterization of fracture features (principal and secondary cracks).

Finite element analysis, even relatively simple, was the more complete of the approaches because it gave the stress distribution not only at the boundaries but also at inner points of the rings, having advantages associated to the numerical calculus. This model has the potential to be enhanced by several ways, reducing the distance between the simulation and the reality, without increasing the mathematical complexity. For example: (a) a finer mesh could be used, including a

higher discretization in the zone of load application; (b) a tridimensional problem could be simulated; (c) the contact area between the rings and the platens (it can be experimentally determined by the impression on the paper) in which the load is distributed could be considered. It is expected that a more realistic estimation of mechanical strength could be obtained if each of these refinements were introduced.

Conclusions

It was possible to study the mechanical resistance of commercially available ceramic rings used as mechanical seals in water pumps, previously characterized by several techniques, employing a non-conventional diametral compression test. Not only the strength was estimated, but also some of the fracture characteristics.

Several approaches, including analytical and numerical models, were used to calculate the fracture resistance values obtaining different results. They also differed in respect to the fracture features that can be predicted from them. The simplest one, an analytical formula that only requires the knowledge of the geometrical magnitudes of rings beside fracture loads, gave a conservative estimation of the mechanical strength of rings and a limited explanation of fracture features. On the other extreme, the numerical model, being the most complex and informative of the approaches, gave complete stress distributions. In addition to the advantages associated to the numerical calculus, it is possible to enhance the model by several ways in order to give more realistic results.

Acknowledgements Suggestions from Ing. J.C. Belmonte and Dr. M.D. Chapetti about analytical and numerical models are gratefully acknowledged. The authors thank Ing. M.D. Echeverría for the roughness measurements.

References

1. Price HL, Murray KH (1973) J Eng Mater Technol 95H:186
2. Vardar O, Finnie I (1975) Int J Fract 11:495
3. Marion RH, Johnstone JK (1977) Ceram Bull 56:998
4. Ozkan N, Briscoe BJ (1997) J Eur Ceram Soc 17:697
5. Bortz SA, Lund HH (1964) In: Kriegel P (ed) Mechanical properties of engineering ceramics. Interscience, New York, p 383
6. Villora JM, Callejas P, Barba MF, Baudín C (2004) J Eur Ceram Soc 24:589
7. Timoshenko S, Goodier JN (1959) In: Theory of elasticity, 2nd edn. McGraw-Hill Book Co., New York, p 116
8. Durelli AJ, Lin YH (1986) J App Mech 53:213
9. Lidering SA Sellos mecánicos-serie standard. Technical Data, Barcelona, Spain
10. Meccanotecnica Umbra Tenute meccaniche frontali-serie FA. Technical Data, Italy
11. Roark R In: Formula for stress and strain, 4th edn. McGraw-Hill Book Company, NY, p 171
12. Frocht MM (1951) In: Strength of materials. Ronald Press, New York, p 175
13. Mari EA (1982) In: Los Vidrios, propiedades, tecnologías de fabricación y aplicaciones. Editorial Americalee, Buenos Aires, p 69
14. Espósito L, Tucci A, Andalo G (1997) J Eur Ceram Soc 17:479
15. Frei H, Grathwohl G (1993) Ceram Int 19:93
16. Gitzen WH (1970) In: Alumina as ceramic material. The American Ceramic Society, Columbus, Ohio
17. Munro R (1997) J Am Ceram Soc 80:1919
18. Mussler BH, Shafer MW (1984) Ceram Bull 63:705
19. Camerucci MA (1999) Ph.D. Thesis, University of Mar del Plata, Argentina
20. Sglavo VM, Pancheri P (1997) J Eur Ceram Soc 17:1697
21. Rice RW (1986) In: Varner JR, Frechette VD (eds) Fractography of glasses and ceramics, vol 22. Advances in Ceramics, The American Ceramic Society, Westerville, p 3
22. Jayatilaka A De S (1979) In: Fracture of engineering brittle materials. Applied Sci. Publishers, Ltd
23. Xu HHK, Wei L, Jahanmir S (1996) J Am Ceram Soc 79:1307
24. Giovan M, Sines G (1981) J Am Ceram Soc 64:68
25. Tomba Martinez AG, Cavalieri AL (2000) Mat Res Bull 35:1077